Fig. 22 displays a comprehensive collection of phase and bifurcation diagrams of the unfolding in Eq. (59). The bottom left subfigure shows the hysteresis surfaces located in the upper half-space $\lambda > 0$ plotted in blue and the upper bifurcation surface plotted in black. The other three subfigures show slices of these surfaces by the planes $\gamma = 1$, $\gamma = 0$, and $\gamma = -1$, along with representative and special bifurcation diagrams of $|u|^2$ versus $\sigma$. Solid green lines represent asymptotically stable intervals, while dashed blue lines depict unstable ones. The stability of the branches was checked using the determinant and trace stability conditions found in Appendix D. Note that the local changes in the bifurcation diagrams $|u|^2$ versus $\sigma$ at the hysteresis and bifurcation singularities match those depicted in Fig. 20.

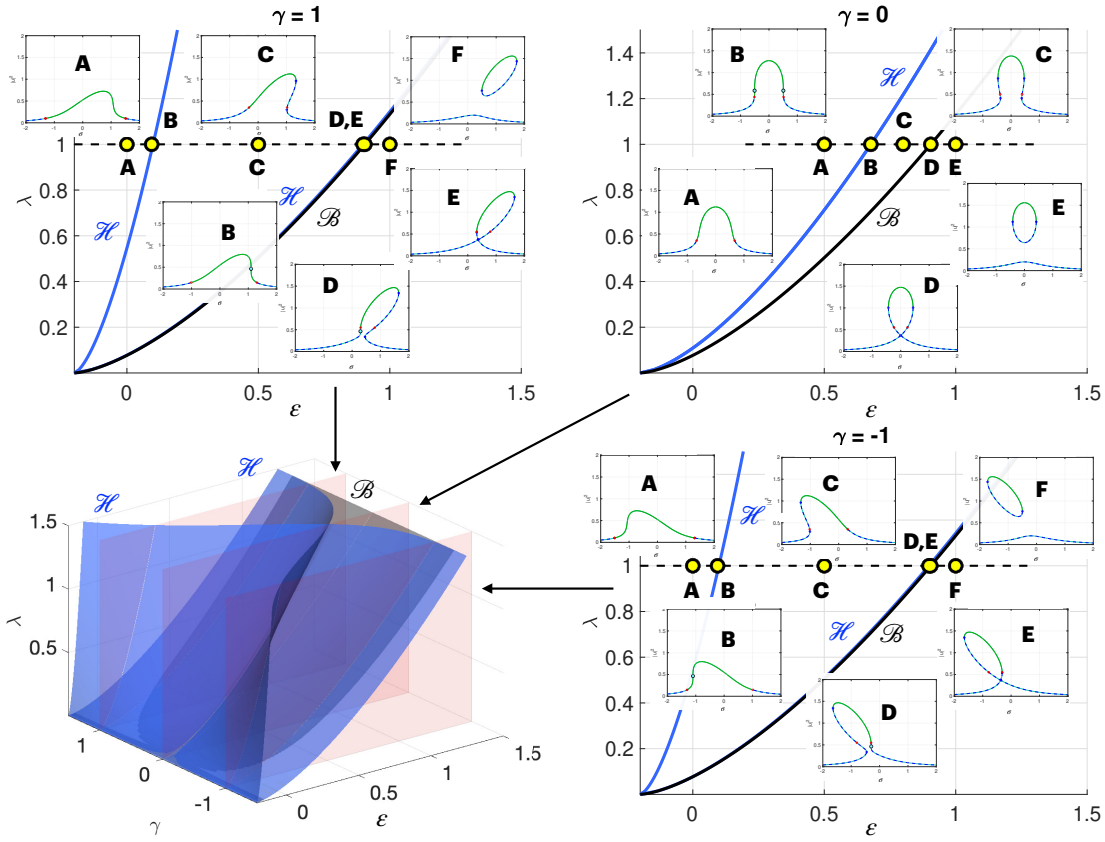


Figure 22: The results of the singularity theory approach applied to system (46). We treat $\sigma$ as the bifurcation parameters, while $\lambda$, $\varepsilon$, and $\gamma$ as the unfolding parameters in Eq. (59). The parameter $\mu$ is fixed at $\mu = 0.2$. The 3D figure in the bottom left displays the hysteresis, $\mathcal{H}$ (blue), and the bifurcation, $\mathcal{B}$ (black), surfaces in the unfolding parameters $(\varepsilon, \gamma, \lambda)$-space. The pink planes correspond to the selected values of $\gamma$: $\gamma = 1$, $\gamma = 0$, and $\gamma = -1$. The sections of the phase diagrams by these planes are shown in the top left, top right, and bottom right, respectively. The blue curves are the hysteresis curves, while the black ones are the bifurcation curves. Note that the black and one of the blue curves are very close at $\gamma = \pm 1$. The insets show the plots of $x \equiv |u|^2$ versus $\sigma$ as fixed $\lambda = 1$, $\gamma \in \{1, 0, -1\}$, and $\varepsilon$ marked by the yellow dots with black edges. The solid pieces correspond to asymptotically stable periodic solutions of system (46), while the dashed ones to unstable periodic solutions. The hysteresis points, marked by cyan dots with black edges, are those with the vertical tangent. The curves $|u|^2$ versus $\sigma$ split into two connected components at the bifurcation points.

### 4.4.1 Reconciling with the phase diagrams for the reduced system

Fig. 23 relates the hysteresis and bifurcation points given by Eqs. (62) and (65), respectively, to the reduced system phase diagrams in the $(\tilde{\sigma}, \tilde{\mu})$-plane in Figs. 10 and 19. The hysteresis

points in Eq. (62) rewritten in terms of $\tilde{\sigma} = \frac{\sigma}{\lambda}\sqrt{\frac{\mu+\varepsilon}{\mu}}$, $\tilde{\mu} = \frac{\mu+\varepsilon}{\lambda}\sqrt{\frac{\mu+\varepsilon}{\mu}}$, and $|v|^2 = |u|^2/(\mu+\varepsilon)$ are:

$$\tilde{\mu} = \frac{3\sqrt{3}}{2\sqrt{2}}\frac{(1 \pm \frac{\gamma}{\sqrt{3}})^{3/2}}{(1+\gamma^2)^{1/2}}, \quad \tilde{\sigma} = \frac{3\sqrt{3}}{2\sqrt{2}}\frac{(\gamma \mp \frac{1}{\sqrt{3}})(1 \pm \frac{\gamma}{\sqrt{3}})^{1/2}}{(1+\gamma^2)^{1/2}}, \quad |v|^2 = \frac{2}{3}\left(1 \pm \frac{\gamma}{\sqrt{3}}\right)^{-1}. \tag{68}$$

One can check that Eq. (68) with $\gamma = 0$ matches the singularity described in Statement 4 of Proposition 1:

$$\tilde{\sigma} \equiv \frac{\sigma}{\lambda} = \pm\frac{3}{2\sqrt{2}}, \quad \tilde{\mu} \equiv \frac{\mu}{\lambda} = \frac{3\sqrt{3}}{2\sqrt{2}}, \quad |v|^2 \equiv \frac{x}{\mu} = \frac{2}{3}. \tag{69}$$

The bifurcation locus with the condition $\frac{4}{27}(\mu+\varepsilon)^3 = \lambda^2\mu$ is equivalent to $\tilde{\mu} = \frac{3\sqrt{3}}{2}$, where $\tilde{\mu} = \frac{1}{\lambda\mu^{1/2}}(\mu+\varepsilon)^{3/2}$ is defined in Eqs. (34) and (49). The corresponding $|v|^2 = |u|^2/(\mu+\varepsilon) = \frac{1}{3}$, and $\tilde{\sigma} = \frac{1}{3}\gamma\tilde{\mu}$. The bifurcation points $(\frac{3\sqrt{3}}{2}, \gamma\frac{\sqrt{3}}{2})$ in the diagram in Figs. 10 and 19 are the highest points on the segments of the dash-dotted green curves between their two cusps corresponding to the hysteresis points.

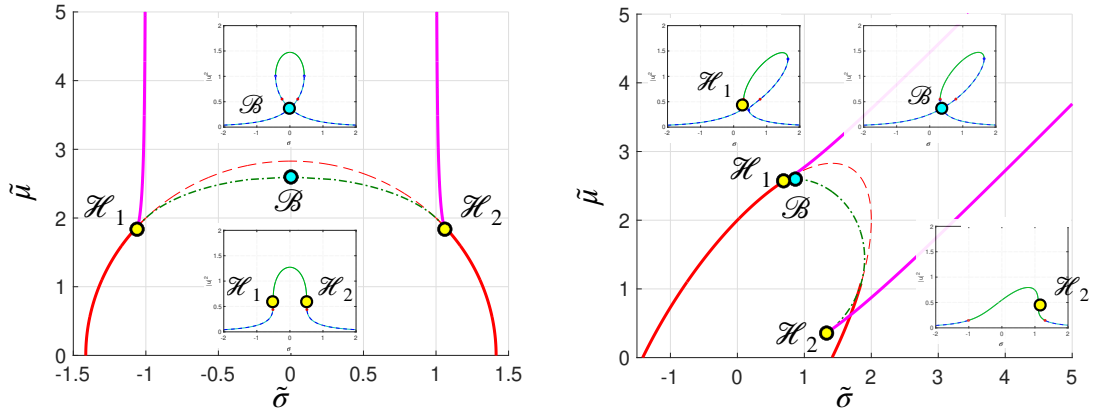


Figure 23: The hysteresis and bifurcation points on the phase diagram for the reduced system (50). The hysteresis points corresponds to the singularities of the curve $\det J = 0$, while the bifurcation points are the highest points of this curve between its singularities. Left: $\gamma = 0$. Right: $\gamma = 1$.

## 4.5 Response amplification in two-cell Stuart-Landau feedforward networks

We have investigated two-cell feedforward networks of inhomogeneous Stuart-Landau oscillators. We now summarize the effects of parameter inhomogeneities on the amplitude of the second cell.

1. **The effect of inhomogeneity in frequency.** The key finding is that the inhomogeneity that fundamentally affects the amplitude of the second cell is the inhomogeneity in frequency, represented by $\sigma$. In particular, if $\gamma = 0$, then the amplitude $|u|$ of the second cell reaches its maximum at $\sigma = 0$. If $\gamma > 0$, the same maximum value of $|u|$ is reached at $\sigma = |u|^2_{\max}\gamma$ – see the insets in Fig. 22.
2. **The range of the phase-locked solution.** Figures 10, 15, and 19 show that the phase-locked attractors persist for a broad range of inhomogeneity in frequency. The region where the phase-locked attractor exists includes the strip

$$|\sigma - \gamma(\mu+\varepsilon)| \le \lambda\sqrt{\frac{\mu}{\mu+\varepsilon}}. \tag{70}$$

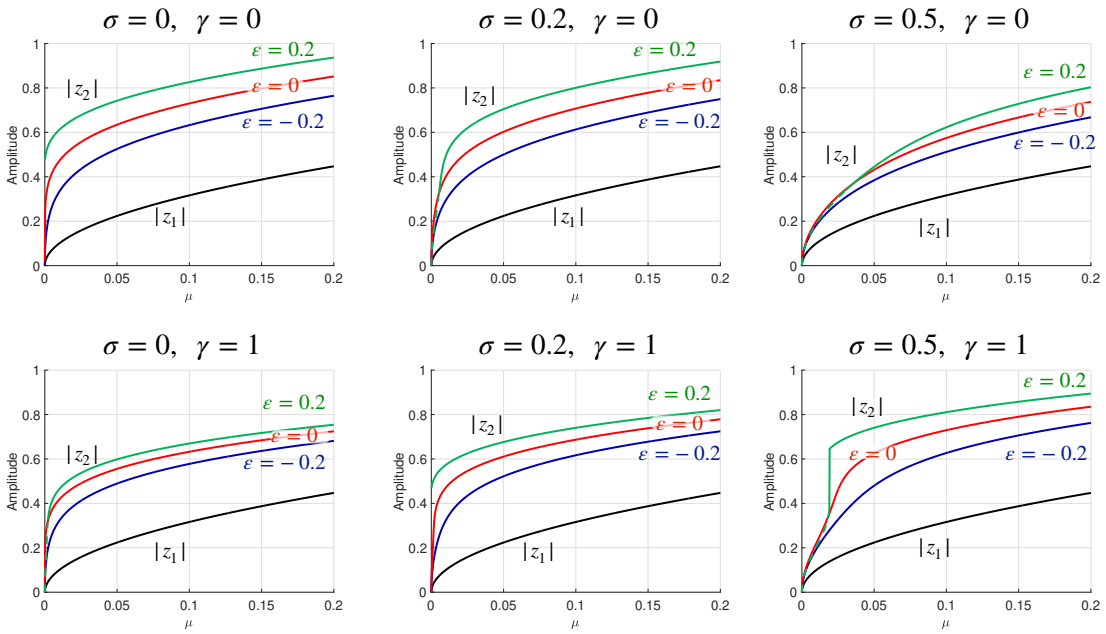


Figure 24: The amplitudes of the cells $z_1$ and $z_2$ of the periodic solutions of system (46) as the functions of $\mu$ at $\sigma \in \{0, 0.2, 0.5\}$, $\varepsilon \in \{-0.2, 0, 0.2\}$, $\gamma \in \{0, 1\}$, and $\lambda = 1$. The black curves depict the amplitude of the first cell, $|z_1|$, while the navy blue, red, and green curves correspond to the amplitude of the second cell, $|z_2| \equiv |u|$ at $\varepsilon = -0.2$, $\varepsilon = 0$, and $\varepsilon = 0.2$, respectively. The solid lines correspond to asymptotically stable periodic solutions, while the dashed lines represent unstable ones. The green curves representing the case $\varepsilon = 0.2$ contain unstable intervals in some cases.

As $\mu + \varepsilon \to 0+$, the interval where the phase-locked attractor exists approaches

$$|\sigma| < \lambda \sqrt{\frac{\mu + \varepsilon}{\mu}} \sqrt{2}. \tag{71}$$

3. **The rapid growth of amplitude at small $\mu$.** Eq. (58) shows that, if $\sigma = 0$, the amplitude $|u|$ of the second cell is approximately equal to $\lambda^{1/3} \mu^{1/6} (1 + \gamma^2)^{-1/3}$ at small $\mu$. This is consistent with the result of [23]. If $\sigma \neq 0$, then $|u| \leq \frac{\lambda^2}{\sigma^2} \sqrt{\mu}$. This rapid amplitude growth is evident in Fig. 24.
4. **The effect of inhomogeneity in the excitation parameter.** If $\varepsilon < 0$, the periodic solution of system (46) is asymptotically stable. The amplitude at the second cell is smaller than its corresponding amplitude at $\varepsilon = 0$ – compare the navy blue and red curves in Fig. 24. In contrast, if $\varepsilon > 0$, the amplitude of the second cell is larger than at $\varepsilon = 0$; however, the periodic solution is unstable at small $\mu$ at $\gamma = 0$ and may be unstable at $\gamma \neq 0$, depending on $\sigma$. This is evident from Fig. 24, where the green curves tend to lie above the red ones, and may have a dashed interval indicating instability of the corresponding solution.
5. **The effect of inhomogeneity in the cubic nonlinearity parameter.** The nonzero $\gamma$ does not affect the amplitude of the second cell. It merely distorts the graph of $|u|^2$ versus $\sigma$, as is evident from the insets in Fig. 22. However, the maximal value of the amplitude shifts away from the center of the stability interval of $\sigma$ as $\gamma$ increases.

# 5 Discussion

Theoretical works [23, 27, 29] reveal that coupling similar nonlinear oscillators in a feedforward fashion can lead, under certain conditions, to accelerated growth rates of amplitudes of